# UV–visible spectral characterization and density functional theory simulation analysis on laser-induced crystallization of amorphous silicon thin films*

Huang Lu(黄 璐)[a)†], Jin Jing(金 晶)[a)], Shi Wei-Min(史伟民)[a)], Yuan Zhi-Jun(袁志军)[b)], Yang Wei-Guang(杨伟光)[a)], Cao Ze-Chun(曹泽淳)[a)], Wang Lin-Jun(王林军)[a)], Zhou Jun(周 军)[b)], and Lou Qi-Hong(楼祺洪)[b)]

[a)] *School of Material Science and Engineering, Shanghai University, Shanghai* 200072, *China*
[b)] *Shanghai Institute of Optics and Fine Mechanics, Chinese Academy of Sciences, Novel Laser Technique and Application System Laboratory, Shanghai* 201800, *China*

(Received 28 May 2013; revised manuscript received 22 August 2013; published online 24 January 2014)

The effect of laser energy density on the crystallization of hydrogenated intrinsic amorphous silicon (a-Si:H) thin films was studied both theoretically and experimentally. The thin films were irritated by a frequency-doubled ($\lambda = 532$ nm) Nd:YAG pulsed nanosecond laser. An effective density functional theory model was built to reveal the variation of bandgap energy influenced by thermal stress after laser irradiation. Experimental results establish correlation between the thermal stress and the shift of transverse optical peak in Raman spectroscopy and suggest that the relatively greater shift of the transverse optical (TO) peak can produce higher stress. The highest crystalline fraction (84.5%) is obtained in the optimized laser energy density (1000 mJ/cm$^2$) with a considerable stress release. The absorption edge energy measured by the UV-visible spectra is in fairly good agreement with the bandgap energy in the density functional theory (DFT) simulation.

**Keywords:** laser crystallization, UV-visible spectra, density functional theory simulation

**PACS:** 42.62.–b, 78.40.–q, 31.15.es, 81.40.Ef **DOI:** 10.1088/1674-1056/23/3/034208

## 1. Introduction

Recently, polycrystalline silicon (poly-Si) films on glass substrates have attracted a great deal of attention in photovoltaics, microelectronics, and display technologies because of their potential applications for electronic devices, such as thin film transistors and thin film solar cells.[1–3] Various crystallization techniques of hydrogenated amorphous silicon (a-Si:H) films can be performed to prepare poly-Si films, such as laser-induced crystallization (LIC),[4–6] metal-induced crystallization (MIC),[7–9] and solid phase crystallization (SPC).[10–12] Due to the minimum thermal damage to the underlying substrates and short processing time, laser-induced crystallization has been extensively used to produce good quality poly-Si films.[13]

However, the traditional crystallization techniques have many shortcomings. With the technique of SPC it is hard to avoid thermal damage to the substrate because the crystallization temperature is too high for the ordinary substrate. With the method of MIC it is difficult to remove the metal impurities from intrinsic materials after crystallization. If the crystalline films are formed into electrical devices later, the metal impurities will affect the properties of devices. Hence, in many recent works green lasers, especially frequency-doubled neodymium-doped yttrium aluminum garnet (Nd:YAG), have been used instead of excimer lasers[14,15] as the crystallization laser source.[16–19] However, crystallization conditions and surface morphology of thin films are very sensitive to the laser energy density.

Therefore, an effective density functional theory (DFT) model can explore the fundamental characteristics of the amorphous silicon materials irradiated by different laser energy densities ($E_L$). Special thermal stress ($\sigma$) is applied to the lattice structure design of amorphous silicon. The simulation model can calculate the bandgap energy ($E_g$) of silicon materials crystallized from the amorphous phase to the polycrystalline phase in different laser energy densities. The results indicate that the bandgap energy values obtained from DFT simulation are in close agreement with the experimental energy values calculated by UV–visible spectral absorption edge. Hopefully, the DFT model studied in this paper may help to prepare a suitable bandgap energy of a-Si:H materials and design an excellent photovoltaic tandem device of thin films by laser-induced crystallization.

In this paper, we focus on the correlation between thermal stress and laser energy density. UV–visible spectral characterization and effective density functional theory (DFT) simulation analysis of thin films after laser crystallization are also investigated.

## 2. Experimental details

Intrinsic hydrogenated amorphous silicon thin films were prepared by the following procedure. First, 200-nm-thick a-

*Project supported by the Shanghai Leading Academic Disciplines, China (Grant No. S30107).
†Corresponding author. E-mail: huanglu@shu.edu.cn
© 2014 Chinese Physical Society and IOP Publishing Ltd 

Si:H films as a layer were deposited on the glass substrates by plasma-enhanced chemical vapor deposition (PECVD) at 250 °C with reactant pressure of 67 Pa–133 Pa. Thin films were prepared using PECVD (HLF-400 system, Beijing Beiyi Innovation Vacuum Technology Co. Ltd., China) by premixing silane ($SiH_4$) with hydrogen ($H_2$) and the volume percentage ratio of $SiH_4$ to $H_2$ was 0.75 vol%. Before the thin films were deposited on the glass substrate, heat-resistant tape had been adhered to the corner of the glass substrate. After we finished depositing a-Si:H thin films and uncovered the tape from the substrate, the thickness of thin film was measured on the step between the glass substrate and thin films by a stylus profiler (Vecco Dektak 150, USA), and then the a-Si:H samples were crystallized using a frequency-doubled Nd:YAG laser. All of the samples were dehydrogenated at $E_L = 100$ mJ/cm$^2$ prior to the laser crystallization in order to prevent ablation of the a-Si:H films.

The a-Si:H thin films were crystallized by a frequency-doubled ($\lambda = 532$ nm) Nd:YAG pulsed nanosecond laser with laser beam shaping system introduced by a fly-eye lens array. The beam-shaping system, including fly-eye lens array, transformed the incoming Gaussian laser beam into a flat top one.[20] The laser could operate at a repetition frequency of 30 Hz and pulse duration of 10 ns. The laser beam by the shaping system was homogenized to a spot of 4 mm×4 mm. The Nd:YAG laser was supported by Shanghai Institute of Optics and Fine Mechanics.

Raman spectra were measured by Jobin Yvon LabHR (HORIBA Co. Ltd., France) Raman spectrometer at room temperature using the 514.5 nm line of an $Ar^+$ laser. The surface morphology of films was determined by atomic force microscopy (AFM). The uncontacted mode of AFM (Park AP-0190, USA) was selected. The grains boundaries had been visualized by anisotropic etching. UV–visible spectra were measured by spectrophotometer (Jasco V-570, Japan).

## 3. Results and discussion

The hydrogenated amorphous silicon thin films were crystallized by a frequency-doubled ($\lambda = 532$ nm) Nd:YAG pulsed nanosecond laser with laser beam shaping system. The laser irradiation can be known to produce a periodic temperature distribution and induce spatially periodic structures on the surface of a-Si film. Therefore, the surface morphology by flat top laser beam differs from the one by Gaussian laser beam. The laser beam is homogenized to a spot of 4 mm×4 mm. Because the melting temperature of a-Si thin films is above 1420 K, the melting region could be transformed to polycrystalline phase.

The characterization by AFM and Raman spectra is also displayed in Fig. 1. In the picture, the poly-Si grain border, grain boundary and polycrystalline grain could be obtained through different Raman shifts. The grain border exhibits a broad peak at about 480 cm$^{-1}$ for a-Si:H (Fig. 1(a)). Exposing the a-Si:H film to polycrystalline grain by laser crystallization, a new peak of crystalline silicon (c-Si) appears at about 520 cm$^{-1}$ corresponding to the transverse optical (TO) phonon for crystalline Si (Fig. 1(b)). The grain boundary shows that its intermediate peak ranges from 480 cm$^{-1}$ to 520 cm$^{-1}$ (Fig. 1(c)).

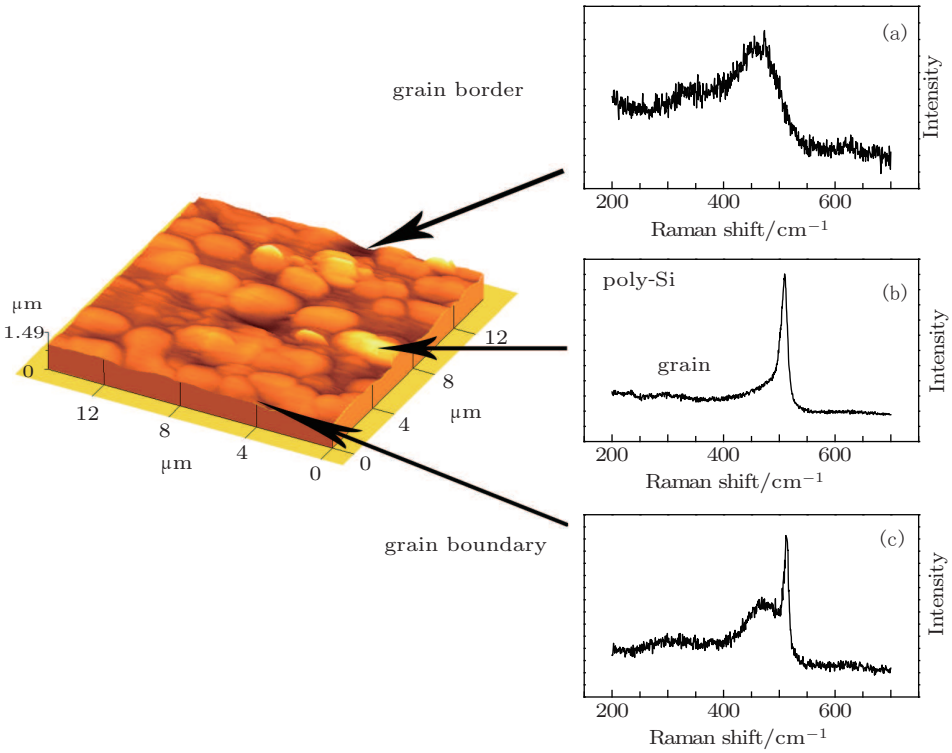



**Fig. 1.** (color online) Surface morphology characterization of a-Si:H thin film on different regions by AFM and crystalline characterization by Raman spectroscopy. (a) Grain border, (b) poly-Si grain, and (c) grain boundary.

To understand the effect of stress on the crystallization process, we have treated the intrinsic a-Si:H films on the glass substrates with laser annealing, as shown in Raman spectra of Fig. 2. The related data of all the films determined from the Raman analysis are displayed in Table 1. The as-deposited a-Si:H ($E_L = 0$) films reveal a broad TO phonon peak at 480 cm$^{-1}$ characteristic for a-Si:H. The TO phonon peak appears at 520 cm$^{-1}$ attributed to crystalline silicon in films at $E_L = 400$ mJ/cm$^2$ and increases with the following steps of laser crystallization sequence at the expense of the amorphous peak. However, the effective crystallization ($X_c = 10.2\%$) occurs in the intrinsic films only at $E_L = 400$ mJ/cm$^2$. Based on Raman spectra, we can infer that the crystallization is strongly enhanced when the laser energy density increases.

The Raman spectra results (shown in Fig. 2) can provide the exact frequency peak of the phonon modes and the corresponding linewidths, as well as a good estimate of the crystalline fraction ($X_c$) in a-Si:H films; $X_c$ is determined from the ratio of the integrated intensities in the TO phonon mode for c-Si to those for a-Si:H. According to the fitting and calculating procedure, the crystalline fraction of $X_c$ is estimated by[21]

$$X_c = (I_c + I_m)/(I_c + I_m + \varepsilon I_a), \quad (1)$$

where $I_c$, $I_m$, and $I_a$ are integrated intensities of c-Si, intermediate and a-Si:H peaks, respectively, $\varepsilon$ is the ratio of Raman cross sections for amorphous to crystalline phase, and in these calculations it is assumed to be 0.9.

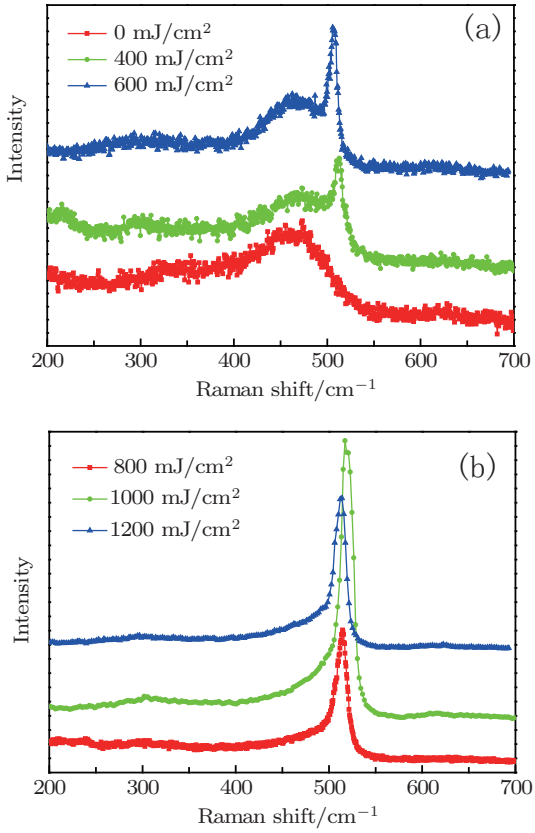



**Fig. 2.** (color online) The Raman spectra characterization of samples by laser crystallization with different laser energy densities. (a) $E_L$=0–600 mJ/cm$^2$, (b) $E_L$=800–1200 mJ/cm$^2$.

**Table 1.** The crystalline fraction ($X_c$), TO peak shift ($\Delta\omega_{TO}$), and thermal stress ($\sigma$) of experimental samples for different laser energy densities.

| Sample No. | Laser power/W | Laser energy density/(mJ/cm$^2$) | $X_c$/% | $\Delta\omega_{TO}$/cm$^{-1}$ | $\sigma$/Pa |
|---|---|---|---|---|---|
| A | 0.1 | 400 | 10.2 | –5.8 | 1.16 |
| B | 0.12 | 600 | 23.4 | –9.1 | 1.82 |
| C | 0.16 | 800 | 44.6 | –3.9 | 0.78 |
| D | 0.2 | 1000 | 84.5 | –1.1 | 0.22 |
| E | 0.24 | 1200 | 71.4 | –5.9 | 1.18 |
| F (baseline) | 0 | 0 | 0 | / | / |

In the intrinsic poly-Si films the peak position of the TO mode for crystalline Si shifts toward lower frequency with respect to 520 cm$^{-1}$ for c-Si as soon as crystallization takes place, indicating the presence of stress in the crystallized films. The determination of stress in crystalline semiconductors by Raman spectroscopy has been investigated extensively. The effect of stress on Raman spectra of Si originates from the lattice deformation, which leads to modified frequencies of the optical phonons. For the case of a uniaxially or biaxially strained silicon layer with an in-plane stress $\sigma$, this correlation is given by[21]

$$\sigma(\text{GPa}) = -0.2\Delta\omega_{TO}(\text{cm}^{-1}), \quad (2)$$

where $\Delta\omega_{TO}$ represents the frequency shift of TO Raman signal at 520 cm$^{-1}$. Following this reasoning, compressive stress ($\sigma < 0$) results in a blueshift of the Raman frequency, while tensile stress ($\sigma > 0$) induces a redshift. Therefore, the Raman spectra confirms tensile stress present in poly-Si films on glass substrates. The TO-related redshifts are obviously observed in thin films and decrease at further laser annealing with improvement of the crystalline quality as suggested by the advent of a sharper Raman peak. Taking into account the mechanical stability of poly-Si thin films on the different solid substrates, the film's stress and structure can determine the performance and reliability of Si-based electronic devices. In order to relieve the stress and improve crystalline quality, the a-Si:H films were obtained. Figure 2 shows the Raman spectra of these films before and after laser annealing. The re-

sults of Raman analysis are summarized in Table 1. The correlations among $X_c$, shift of TO Raman peak ($\Delta\omega_{TO}$) and the respective tensile stress ($\sigma$) provided by Eq. (2). With the improvement in laser energy densities, the Raman TO peak for crystalline Si becomes dominant and the TO-related redshift variation shows an initial increase followed by a decrease with improvement of the crystalline quality, which also occurs in thin films. In particular, the redshifts of TO Raman peaks in the poly-Si films attain considerable decrease, which indicates that much stress release occurs. This demonstrates that the improvement in short-range order (SRO) and decreased disorder effect are apparent for the a-Si:H films, which is also exhibited in laser-crystallized films based on Table 1.

From Fig. 3, $X_c$ seems to be determined by the stress present in the films. The relatively high tensile stress values at 1.16–1.82 GPa limit $X_c$ to 44.6%. After laser annealing at $E_L = 1000$ mJ/cm$^2$, the highest crystalline fraction of $X_c = 84.5\%$ can be obtained by a considerable stress release with the value down to 0.22 GPa. With further increase in the laser energy density, the laser irradiation damage on the films and defect structures induced by laser annealing contribute to the high surface roughness, which would lead to the poorer crystalline quality ($X_c$ down to 71.4%) with the stress value up to 1.18 GPa.

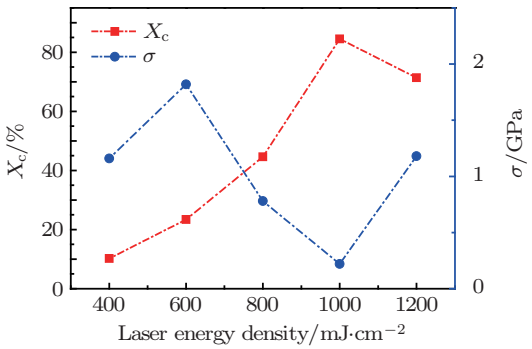



**Fig. 3.** (color online) Crystalline fraction ($X_c$) and the respective tensile stress ($\sigma$) of the a-Si:H thin films crystallized by different laser energy densities.

It is well known that a power law is suitable for an approximation of an optical absorption spectrum at the fundamental absorption edge when the absorption is high. The formula is written for the absorption spectra as[22]

$$(\alpha h\nu) \sim (h\nu - E_g)^r, \tag{3}$$

where $E_g$ is the vertical separation between valence and conduction bands (optical gap), $r$ is the power law index. The value of $r$ is defined by the origin of the optical transitions in the vicinity of the fundamental absorption edge in the crystalline material. Typical absorption spectra at the edge are illustrated for thin films. The absorption spectra are calculated from the experimental results according to the simple relationship

$$\alpha = -\frac{1}{d}\ln\frac{T}{(1-R)^2}, \tag{4}$$

where $d$ is thickness of thin film, $T$ is transmission and $R$ is reflection. $E_g$ was determined from the Tauc plot of the absorption coefficient, $\alpha$ against photon energy $h\nu$ using the following relationship:[23]

$$(\alpha h\nu)^{1/2} = K(h\nu - E_g), \tag{5}$$

where $K$ is a factor independent of $\nu$. $E_g$ is then obtained as the intercept of the curve of $(\alpha h\nu)^{1/2}$ versus $h\nu$, $E_g$ for a-Si:H thin film is measured. The absorption spectra obtained fitted the power law perfectly with the index $r = 2$. It is known that the absorption originates from the indirect-forbidden transitions of electrons between the valence and the conductance bands when the index $r$ is equal to 2.

In Fig. 4, the values of $E_g$, estimated by extrapolating the linear portion of the curve to $(\alpha h\nu)^{1/2} = 0$, are about 1.7 eV, 1.5 eV, and 1.1 eV for amorphous, micro-crystalline and crystalline silicon thin films of 200-nm thickness respectively. The laser energy densities corresponding to amorphous, micro-crystalline and crystalline phase are as-deposited, 600 mJ/cm$^2$ and 1000 mJ/cm$^2$ respectively.

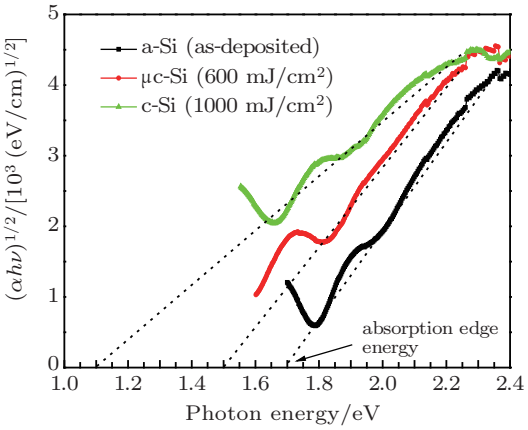



**Fig. 4.** (color online) The UV–visible spectra results (absorption edge energy) of a-Si:H thin films for different laser energy densities.

In the DFT simulation, the physical properties of the semiconductor materials are investigated in detail because they are closely related to the characteristics of the thin film materials. Moreover, the bandgap energy is not only one of the most important properties that influence the absorption wavelength, but also the key point to crystalline quality. Hence, comparing all physical properties obtained from simulation with the experimental values reported by other researchers,[24] the Castep simulation software is used to explore the energy band gaps of the a-Si:H thin film materials by laser-induced crystallization.

In order to obtain the bandgap energy of thin film materials irradiated by different laser energy densities, several different parameters are used to find out the optimal laser energy density. As a result, the bandgap energies of crystalline,

amorphous and polycrystalline silicon are obtained from DFT simulation. We choose to simulate samples of external stress 1.82 GPa crystallized at $E_L = 600$ mJ/cm$^2$, a-Si:H without laser annealing and crystalline silicon ($E_L = 1000$ mJ/cm$^2$), respectively, to investigate the difference in several bandgap energies of silicon thin films. The DFT simulation results in Fig. 5 show that the $E_g$ values of crystalline, amorphous, and micro-crystalline (total external stress 1.82 GPa) silicon are respectively 1.096 eV, 1.64 eV, and 1.482 eV. The related theoretical parameters and structural characteristics are listed in Table 2.

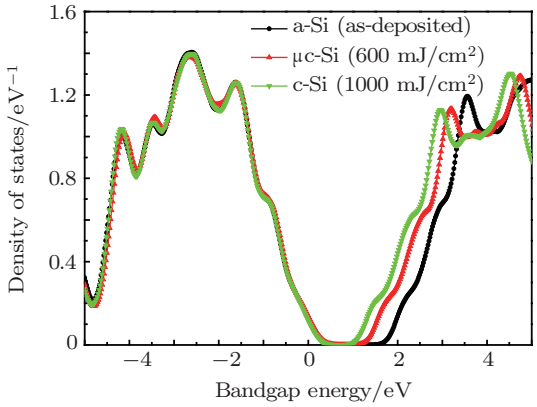



**Fig. 5.** (color online) The DFT simulation (bandgap energy) of a-Si:H thin films for different laser energy densities.

**Table 2.** The related parameters and structural characteristics of DFT simulation.

| Physical parameters | c-si | a-si | μc-Si |
|---|---|---|---|
| Crystal system | cubic | triclinic | triclinic |
| Crystal class | M–3M | P1 | P1 |
| Lattice length $a$/Å | 5.4307 | 3.840085 | 3.840085 |
| Lattice length $b$/Å | 5.4307 | 3.840085 | 3.840085 |
| Lattice length $c$/Å | 5.4307 | 3.840085 | 3.840085 |
| Lattice angle $\alpha$/(°) | 90 | 60 | 60 |
| Lattice angle $\beta$/(°) | 90 | 60 | 60 |
| Lattice angle $\gamma$/(°) | 90 | 60 | 60 |
| External stress $x$ axis/GPa | / | / | 1.05 |
| External stress $y$ axis/GPa | / | / | 1.05 |
| External stress $z$ axis/GPa | / | / | 1.05 |
| Total external stress/GPa | / | / | 1.82 |
| Bandgap energy | 1.096 | 1.640 | 1.482 |

In the experiment of a-Si:H thin films by laser-induced crystallization, the TO peaks in Raman spectra and the calculated $X_c$ reach the maximum value, $\sigma$ reaches the minimum value when the laser energy density is about 1000 mJ/cm$^2$. From Figs. 4 and 5, the bandgap energy of the DFT simulation results accords well with the value of absorption edge energy obtained from the UV–visible spectral results.

## 4. Conclusions

In this paper, the laser-induced crystallization of a-Si:H is numerically and experimentally investigated. The DFT simulation model is used to predict the optimum crystalline conditions, including the critical laser energy density and the bandgap energy for different crystalline phases. The highest crystalline fraction ($X_c = 84.5\%$) and the lowest thermal stress ($\sigma = 0.22$ GPa) are achieved by optimized laser energy density of about 1000 mJ/cm$^2$ in the experiment. The UV–visible spectral characterization of thin films from absorption edge energy for different laser energy densities accords very well with the values of bandgap energy in the DFT simulation results.

## References

[1] Fortunato G 1997 *Thin Solid Films* **296** 82
[2] Mahan A H 2003 *Sol. Energy Mater. Sol. Cells* **78** 299
[3] Brotherton S D 1995 *Semicond. Sci. Technol.* **10** 721
[4] Izawa Y, Tokita S and Fujita M 2009 *J. Appl. Phys.* **105** 064909
[5] Kamenev B V, Grebel H and Tsybeskov L 2006 *Appl. Phys. Lett.* **88** 143117
[6] Wang D Q, Chen G R and Huang X F 2010 *Acta Phys. Sin.* **59** 5681 (in Chinese)
[7] Tang Z X, Shen H L and Huan H B 2009 *Thin Solid Films* **517** 5611
[8] Tao Y L, Zuo Y H and Zheng J 2012 *Chin. Phys. B* **21** 077402
[9] Wu Y, Jing H and Ma K 2006 *Chin. Phys.* **15** 1310
[10] Xu H J, Chan Y F and Su L 2011 *Chin. Phys. B* **20** 107801
[11] Mudugamuwa N K, Dissanayake D M N M and Adikaari A A D T 2009 *Sol. Energy Mater. Sol. Cells* **93** 549
[12] Park J H, Kim D Y and Ko J K 2003 *Thin Solid Films* **427** 303
[13] Voutsas A T 2003 *Appl. Surf. Sci.* **208–209** 250
[14] Chen Y R, Chang C H and Chao L S 2007 *J. Cryst. Growth* **303** 199
[15] Rezek B, Nebel C E and Stutzmann M 2002 *J. Appl. Phys.* **91** 4220
[16] Akito H, Fumiyo T and Michiko T 2002 *Jpn. J. Appl. Phys.* **41** 311
[17] Dassow R, Kohler J R and Helen Y 2000 *Semicond. Sci. Technol.* **15** 31
[18] Park S J, Ku Y M and Kim E H 2006 *J. Non-Cryst. Solids* **352** 993
[19] Saboundji A, Mohammed B T and Andra G 2004 *J. Non-Cryst Solids* **338–340** 758
[20] Yuan Z J, Lou Q H and Zhou J 2009 *Opt. Laser Technol.* **41** 380
[21] Jin J, Yuan Z J and Huang L 2010 *Appl. Surf. Sci.* **256** 3453
[22] Galdikas A, Mironas A and Senulienc D 1998 *Thin Solid Films* **323** 275
[23] Shen Y, Tao J C and Gu F 2009 *J. Alloys. Compd.* **474** 326
[24] Yamaguchi M, Ogihara C and Morigaki K 2003 *Mater. Sci. Eng. B* **97** 135